Pattern Anal Applic (2015) 18:277–295
DOI 10.1007/s10044-013-0342-x

THEORETICAL ADVANCES

Accurate object detection using local shape descriptors

Mohammad Anvaripour · Hossein Ebrahimnezhad

Received: 1 April 2012 / Accepted: 24 May 2013 / Published online: 3 July 2013

Abstract This paper proposes a novel object detection approach based on local shape information. Boundary edge fragments preserve some features like shape and position which properly describe the outline of an object. Extraction of object boundary fragments is a challenging task in object detection. In this paper, a sophisticated system is proposed to achieve this goal. We propose local shape descriptors and present a boundary fragment extraction method using Poisson equation properties, and then, we compute relation between boundary fragments using GMM to obtain exact boundaries and detect the object. To get more accurate detection of the object, we employ a False Positive elimination stage based on local orientation histogram matching. The proposed object detection system is applied on several datasets containing object classes in cluttered images in various forms of scale and translation. We compare our approach with other similar methods that use shape information for object detection. Experimental results show the power of our proposed method in detection and its robustness in face with scale and translation variations.

Keywords Object detection · Shape-based features · Poisson equation · False Positives elimination · Generic model

M. Anvaripour · H. Ebrahimnezhad (✉)
Computer Vision Research Laboratory, Electrical Engineering Faculty, Sahand University of Technology, Tabriz, Iran
e-mail: ebrahimnezhad@sut.ac.ir

M. Anvaripour
e-mail: m_anvaripour@sut.ac.ir

1 Introduction

Object detection is of fundamental importance in the computer vision and has received a great deal of attention in the recent years. Detection is the process of localizing and finding the scale of an object in an image. Humans find objects in a scene by considering their shapes. So, shape information is a significant cue for object detection. Shape of objects can be inferred from the shape of boundary edges or contours [1, 2]. While extracting sufficient shape information still poses a large challenge, recent research in detection allows extraction of local shape hypotheses.

In this paper, object descriptors are introduced as a means of acquiring the object shape, configuration, and model. Poisson equation properties are employed to extract local features from edge image. Besides, boundary fragments and local orientations of objects are utilized as local features. Characteristics of boundary fragments are collected in a class-specific codebook as a set of their local orientations, scales, and positions according to the object center. Object configuration is defined as the relation between boundary fragments [3, 4]. Models are typically identified as sparse collection of local features [5]. Gaussian mixture model (GMM) is utilized to develop the object configuration as a complete graph. A generic model is created and histograms of local orientations for desired object are acquired for shape matching purpose.

The challenge is to find the object boundaries for detection purpose. To extract the object boundaries from edge points, some characteristics of edge fragments including pose, local orientation and scale are employed. To derive an automatic initialization for the location, scale, and probable boundaries of the object, a Hough style voting scheme [6] is implemented, which enables us to match the object shape in database with severely cluttered images,

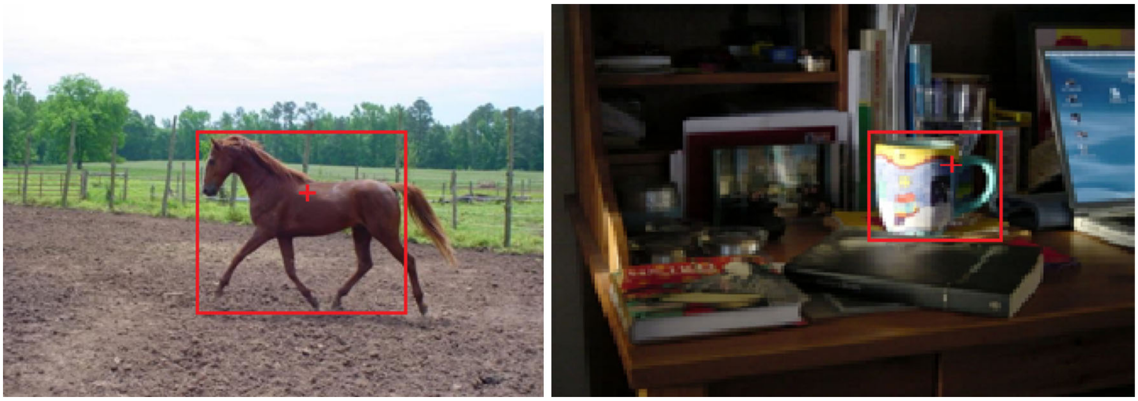

Fig. 1 Two examples of detected objects by the proposed method

where the object boundaries cover only a small fraction of the edge points [7]. A Mean-Shift algorithm is also used to find the local maxima and center of the object. In cluttered images, some edges may be established as a part of object boundary, incorrectly. To alleviate the problem, a trained GMM is applied to find relation between the established boundary fragments and launch the shape of object.

False Positive is a usual problem in detection tasks, which occurs when incorrect objects are detected. In this paper, a False Positive elimination procedure is proposed by matching the histogram of local orientation of the model with the extracted shape of object using Poisson equation properties. Histogram of local orientation gives a description of object shape and helps us to find the object accurately and remove false detections. Some examples of detected objects by our approach are shown in Fig. 1 in which a bounding box covers the object boundaries. Figure 2 illustrates the stages of our proposed method. A preliminary version of this work has appeared in [8]. The remainder of this paper is organized as follows. In Sect. 2, the related studies of shape-based object detection are presented. Section 3 introduces our proposed object descriptors. In Sect. 4, the object detection stage is described. Section 5 reports extensive experiments in which our method has been evaluated and compared with the previous studies. Finally, the conclusion of the paper appears in Sect. 6.

2 Related works

Our method relies on localizing and finding the scale of the object by considering its shape information. Shape of object can be acquired using boundary edges or contours [1] and segmentation methods [9]. This section concentrates on the most related studies that employ some concepts of geometry or shape for various object classification tasks in an image.

Contour was first used for template matching to detect objects [10–12]. In [11], chamfer matching is used to find proper contours. An alternative method is using of contour fragments or boundary edge fragments as presented in [1, 13]. Authors of these papers used contour fragments as local features of object boundaries and employed Hough voting space for detection. A boosting algorithm is used to train the shape and position of fragments in the coordinate of object center. In [13], region of interest in image is obtained by the searching algorithm presented in [14]. This algorithm seeks regions for the most probable presence of the object center according to contour fragments.

In some studies, edge points have been used as an attractive feature. In [15], the number of edge points in a region was used as a feature for shape representation. Sampling edges and the relations between them are used in some methods. In [7], a model is constructed using fragments in the extracted codebook. Boundary of the model is discretized to uniform samples of points. These points are matched with extracted points in the image by TPS-RPM algorithm that was presented in [16] for non-rigid shape matching. In [17], geometric blur [18] is used as an operator for sampling the edges. Landmarks were introduced in [19] to split boundaries and edges. In [19], Markov random field has been proposed for modeling the shapes of the objects in a variety of object poses using landmarks.

In [20], the edges of input image are partitioned into contour segments and organized in an image representation as contour segment network. The object detection problem is treated by finding paths through the network resembling the model boundary. The network is created by connecting contour segments. This approach of connecting the segments has been used by the same authors in their next study. They present KAS features for detection in [21] and use SVM classifier to train an explicit shape of the object and detect it.

Although object detection through edges was used in many studies, the proper object boundary and object shape may not be obtained in cluttered images. To this end, graphs have been used as they are useful for perfect localizing and extracting the shape of an object. The relation between local features such as graphs demonstrates object structures. In [22], a geometrical arrangement of parts was computed to make an explicit shape model of the object. Most of these models have been developed to increase the accuracy of recognition or classification, rather than to accurately localize the constituent parts or the objects [19]. However, such models can be developed for object localization through local edges or contour fragments.

The relation between local features induces False Positives in some clutter images, which can be fairly removed by employing shape information. Shape of the object can be obtained by class-based segmentation. Shape information, existing in the image in the form of coherent image regions or segments and their bounding contours, provides a strong cue that can be used for detection [25]. In [9, 23], images are segmented based on class-specific image features for the class-based segmentation of the relevant object class. These approaches, however, aim to maximize the region of interest. Bottom-up segmentation is presented in [24], which combines tiny segments to form larger regions. In [25], Poisson equation is solved for a big region with a tall effective boundary to describe shape of the region and to find proper segments of the desired object. Poisson equation has been presented in [26] for shape classification. Solution of Poisson equation at a point in the interior of a region represents the average time required for a particle to hit the boundary at a random walk starting at a specific point. Such a solution allows the smooth propagation of contour information of a region to every internal pixel [26]. Poisson equation has several useful properties that can be used for detection and classification tasks.

In this paper, we propose a sophisticated object detection system by extracting object boundaries, constructing object configuration, and making generic models including histograms of local orientation of the objects to enhance the removal of False Positives in cluttered images. The proposed method has the better detection performance in face with troubling edge fragments compared to state-of-the-art methods. Enjoying a high detection performance, our method removes the False Positives. In the following sections, the two main parts of the proposed approach including object descriptor and detection task are introduced.

3 Object descriptor

Our detection process is based on shape properties of objects, in which the shape is identified using boundary fragments and local orientations of the object. Boundary fragments are used to expose presence of the object in the image, and local orientation of the object parts are used to match the local shape descriptor to obtain the nearest shape to the model and overcome False Positives. The proposed object descriptor is generated in three steps: creating codebook from local boundary fragments, making object configuration, and constructing generic model descriptor. In the following subsection, the proposed object descriptor has been described in detail (left part of Fig. 2 illustrates object descriptor extraction process).

3.1 Codebook creation from local boundary fragments

Object boundaries are the best features for describing object shape that are invariant to color and brightness changes in images. However, it is difficult to extract object boundaries thoroughly in natural images. Therefore, we use local boundary fragments as the primitive descriptors and store them in a class-specific collection called codebook.

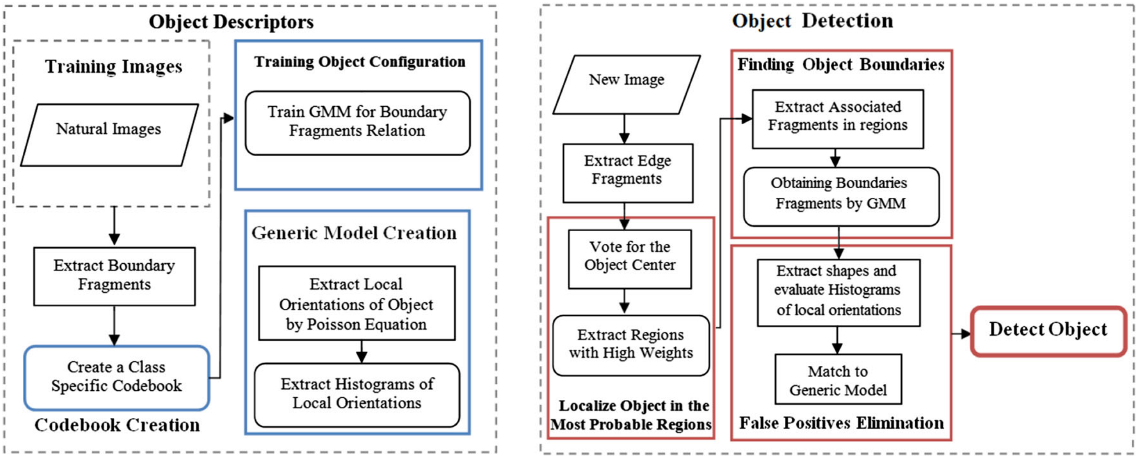

Object Descriptors
Training Images
Natural Images
Extract Boundary Fragments
Create a Class Specific Codebook
Codebook Creation
Training Object Configuration
Train GMM for Boundary Fragments Relation
Generic Model Creation
Extract Local Orientations of Object by Poisson Equation
Extract Histograms of Local Orientations
Object Detection
New Image
Extract Edge Fragments
Vote for the Object Center
Extract Regions with High Weights
Localize Object in the Most Probable Regions
Finding Object Boundaries
Extract Associated Fragments in regions
Obtaining Boundaries Fragments by GMM
Extract shapes and evaluate Histograms of local orientations
Match to Generic Model
False Positives Elimination
Detect Object

Fig. 2 Overview of the proposed method

At the beginning of feature extraction process, we find edge points of the images using canny edge detector and split them from junction points. These edges are still raw and insufficient to explain shapes of the objects in images. To get a more descriptive shape feature, we use the solution of Poisson equation on these raw edges. Poisson equation has several properties that are introduced in [26]. It can be used to extract a wide variety of useful properties of a silhouette binary image including segmentation of a silhouette into parts, identifying corners at various resolution scales, deriving a skeleton structure, and locally judging the orientation. Poisson equation is solved on a binary edge image. Equation (1) presents this equation in which U refers to the solution of the equation:

$$\nabla^2 U = -1 \tag{1}$$

The concept of Poisson equation can be considered as a set of particles that have random walk originated from a point. Some statistics of this random walk can be measured such as mean time required for a particle to hit the boundary [26]. The numerical solution presented in [26] is multigrid algorithm, because of the fast process of this algorithm. In multigrid solution, the residual equation is solved and averaged to represent them on a coarse grid where the distance between neighborhoods grids is twice the fine grid distance. The solution is interpolated to the fine grid to have a good approximation for the smooth error and correct the previous solution. This kind of relaxation that is followed by a correction is called multigrid cycle. This equation is solved under Dirichlet boundary condition considering $U(x,y) = 0$ at the object contour in binary image. The solution of the Poisson equation is very robust in noisy boundaries, especially after relaxation sweep, discussed in [26]. To reduce the noise near the boundaries, a post processing stage is applied that solves the equation $U_{xx} + U_{yy} = -1$ inside and $U_{xx} + U_{yy} = 0$ outside the object in a binary image.

The Poisson equation can be also used to estimate the local orientation of a shape. So, we compute the local orientation of each edge fragment by employing the Poisson equation solution. Local orientation is computed by Hessian matrix of U in each edge point. The Eigen vector that corresponds to the smaller Eigen value of Hessian matrix in an edge point is considered as the local orientation of the edge in that point. Local orientations which are obtained by explained procedure describes edge orientation variation smoothly and more precise than other methods such as gradient. Equation (2) shows the Hessian matrix of U at pixel (x, y):

$$H(x,y) = \begin{bmatrix} \frac{\partial^2 U}{\partial x^2} & \frac{\partial^2 U}{\partial x \partial y} \\ \frac{\partial^2 U}{\partial y \partial x} & \frac{\partial^2 U}{\partial y^2} \end{bmatrix} \tag{2}$$

We split edges from the high curvature points after computing their local orientations and present each fragment by three parameters: fragment length, orientation of the left part (L), and orientation of the right part (R). Orientation of each part is quantized into six values (−π/3, −π/6, 0, π/6, π/3, π/2); therefore, each edge fragment will acquire one of the 36 possible forms of the L–R orientations.

To achieve the boundary fragments, we use a set of natural images in which the interested object is surrounded by bounding boxes. Before extraction of boundary fragments, we resize the bounding boxes in different images to a fixed size to get a scale invariant model. After extraction of edge image from each image in dataset inside the bounding box, it is decomposed to 36 different oriented edge image layers based on the status of L–R orientation of the edge fragments. So, each oriented edge image layer will contain only the edge fragments with special orientation. For example, the first and second layers contain the edge fragments with the L–R orientations of (−π/3,−π/3) and (−π/3,−π/6), respectively. As a general rule, the $(i \times j)$th layer contains the fragments with the L–R orientation of (θ_i,θ_j), where θ_i and θ_j belong to the angle set ($\theta_1 = -\pi/3$, $\theta_2 = -\pi/6$, $\theta_3 = 0$, $\theta_4 = \pi/6$, $\theta_5 = \pi/3$, $\theta_6 = \pi/2$).

As we know, the boundary fragments follow the shape of the object. Supposing that the objects are surrounded by the bounding boxes in all dataset images and they are scaled to have equal sizes, thus, we can aggregate the similar layers of edge fragments in different images of one object class to separate boundary fragments from other fragments. In fact, in the aggregated image of the similar layers, we will find a large number of fragments in the location of boundaries because of the same length and orientation of such fragments. In the other words, boundary fragments of an object in different images appear in a same position with respect to the center of bounding box. Any location in the aggregated image, which contains boundary fragments, holds the large number of edge points, because of the regular shape of such fragments. On the contrary, any location of non-boundary fragments holds the small number of edge points the aggregated image (because of the random shape of such fragments). In consequence, we can separate boundary fragments from other edge fragment and store them in a codebook. For each boundary fragment, a feature vector $\boldsymbol{F}$ defined in Eq. (3) is assigned and all of the vectors are stored in a codebook as the possible boundary fragments of the object.

$$F = [\theta_\mathrm{l}, \theta_\mathrm{r}, S, x, y] \tag{3}$$

In this equation, θ_l and θ_r are the orientation of left and right parts of boundary fragment, S is the length (or scale) of the boundary fragment, and (x, y) show the pose of the fragment center (the joint point of left and right parts) with respect to the object center. Figure 3 illustrates an example of extracted boundary fragment for swan image.

The created codebook in training stage includes all kind of possible boundary fragments of the object in different image samples of object in dataset. In the test stage, we should compare feature vector of any edge fragment with the samples of codebook to verify whether it is a boundary fragment or not. Therefore, the candidate boundary fragments of test image are held and the other troubling edges are removed. To simplify the seeking process of the edge fragments in the codebook for the test image, we do the matching in a hierarchical method. To achieve this end, we cluster the codebook entries according to their orientation $(\theta_{\mathrm{l}}, \theta_{\mathrm{r}})$, length (S) and position (x, y). For this purpose, we consider a rectangular region in the neighborhood of each boundary fragment center in the aggregated images and compute average orientation $\left(\theta_{\mathrm{l}}^r, \theta_{\mathrm{r}}^r\right)$, average length (S_r) and average position $(x_r,\ y_r)$ for the fragments that their centers are posed inside the region. Figure 4 shows an example of code creation for swan. In the upper side, the edge fragments of 8 swan images are shown. In the bottom side, 4 arbitrary layers of aggregated images (from 36 layers) are shown. In the aggregated images, there are some regions with a large number of edge points (the yellow rectangles) that show the local boundary fragments of the object. These regions are clustered according to their pose, angle, and length as mentioned above and feature vector of the center of clusters are defined as $F^r = [\theta_{\mathrm{l}}^r, \theta_{\mathrm{r}}^r, S_r, x_r, y_r]$.

To get more exact boundary fragments and remove the false fragments from codebook, we compute the distance of feature vector of each entry of codebook (F^a) from cluster centers (F^r) using Eq. (4):

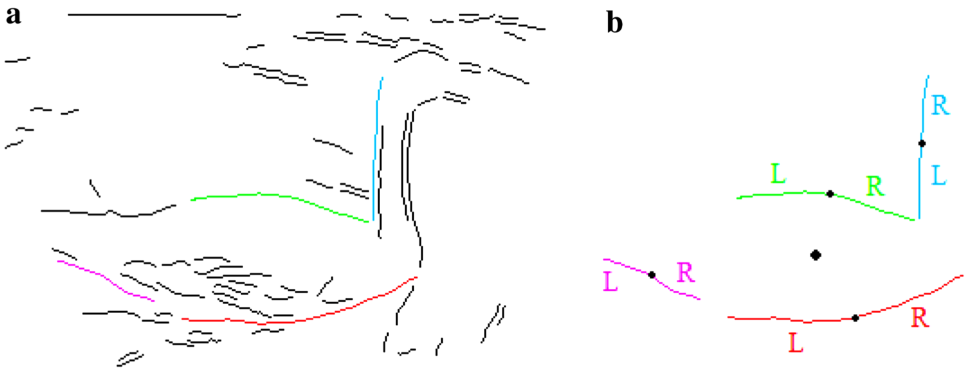

Fig. 3 Edge fragments of an image. **a** Edge fragments of a swan image, with four boundary fragments of swan, **b** four sample fragments extracted from image. *Blue*, *green*, *red* and *magenta* fragments have orientations [90, 90], [0, −30], [0, 30] and [−30, −60], respectively (color figure online)

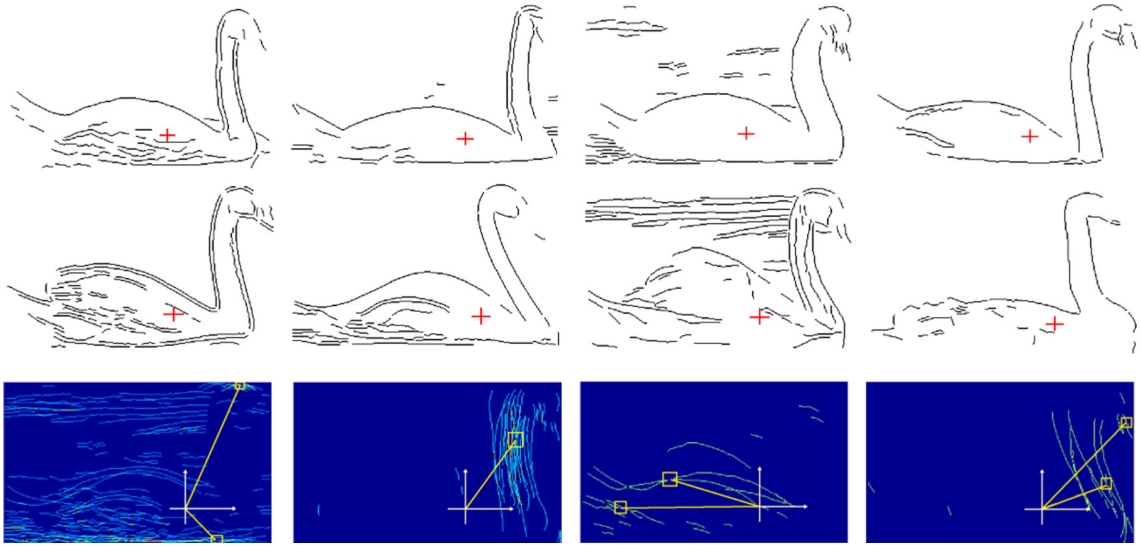

Fig. 4 Codebook creating. Eight images of the edge fragments of swans and four sample images of aggregated fragments. *Red plus*, +, indicates the center of the object, *Yellow rectangles* denotes the high weight locations and local boundary fragments. *Yellow lines* show the pose of local edge fragments relative to the center of object that is obtained by averaging center of the object in above eight images. Center of object is identified by *white axis* (color figure online)

$$D(F^r, F^a) = w_\theta \cdot \left(1 - \frac{\left\langle \vec{\theta}^r, \vec{\theta}^a \right\rangle}{\left\|\vec{\theta}^r\right\| \left\|\vec{\theta}^a\right\|}\right) + \left|\log\left(\frac{S_r}{S_a}\right)\right| + \frac{1}{\mathrm{Diag}} \cdot \sqrt{(x_r - x_a)^2 + (y_r - y_a)^2}$$
$$= w_\theta \cdot \left(1 - \frac{\theta_1^r \theta_1^a + \theta_\mathrm{r}^r \theta_\mathrm{r}^a}{\sqrt{(\theta_1^r)^2 + (\theta_\mathrm{r}^r)^2}\sqrt{(\theta_1^a)^2 + (\theta_\mathrm{r}^a)^2}}\right) + \left|\log\left(\frac{S_r}{S_a}\right)\right| + \frac{1}{\mathrm{Diag}} \cdot \sqrt{(x_r - x_a)^2 + (y_r - y_a)^2} \tag{4}$$

In this equation, F^a is a feature vector of fragment a in the codebook. At the first term of the equation, the orientation difference of two fragments is computed. The second term calculates the logarithm difference between the lengths (scales) of two fragments. Finally, the third term determines the Euclidean distance between locations of the fragments. Diag is the diagonal length of training image (or the bounding box of object), which is used for normalization. x_a and y_a determine the position of the center of the fragment. We set $w_\theta = 2$ in our experiments to indicate the importance of the orientation in the shape similarity computation. Under the condition that $D(F^r, F^a) < 0.01 \times \mathrm{Diag}$, the fragment F^a is counted as cluster F^r in the codebook.

The generated codebook is adequate for the matching process because all the features in the codebook clusters have specific scales and angles and represent spatial transformation of the fragments according to the center of the object. By this way, the sequential form of fragment matching can be converted into the hierarchical form in which we find the similar cluster at first and find the exact entry of codebook at final. Therefore, the matching process will be easy and fast.

3.2 Object configuration

Relationships between the local features are important shape cues that can be used in recognition and detection of the object. Since extracting the complete shape of an object in the cluttered natural images is impractical, relation between the local features or graphs [27] helps us to recognize the object by indicating configuration of the local features. In this paper, we deal with object configuration through the relationships between its boundary fragments stored in the codebook as a complete graph. We use such relationships to find the true boundaries of the object from the candidate boundary fragments obtained from the codebook matching stage. Since, distribution of such local features cannot be considered as a Gaussian function, combination of two or more Gaussian functions gives more precise representation of feature distribution. Thus, the relations between these local features are constructed using GMM.

We use the boundary fragments in the codebook clusters. First, for each cluster in the codebook, we select the edge fragment in the average length and the average distance from the object center as a representative fragment. Then, we construct the relation between these local features using GMM.

Let $\lambda = \{w_i,\ \mu_i,\ \Sigma_i,\ i = 1 \ldots N\}$ be the set of the parameters of a GMM, where w_i, μ_i and Σ_i denote weight, mean, and covariance of Gaussian function i. If q be the hidden mixture variable associated with the observation O, then:

$$p(O|q) = \sum_{i=1}^{N} w_i p(O|q = i, \lambda), \tag{5}$$

with:

$$p(O|q = i, \lambda) = \frac{1}{2\pi^{\mathrm{D}/2}|\Sigma_i|^{1/2}} \cdot \exp\left\{-\frac{1}{2}(O - \mu_i)^T \Sigma_i^{-1}(O - \mu_i)\right\} \tag{6}$$

where, D is the dimension of observation vector.

To train the object configuration using GMM, we use training samples $O = \{o_t,\ t = 1 \ldots T\}$, as a collection of T observations. Estimation of λ can be performed by maximizing the log-likelihood function log $p(O|\lambda)$. Each sample is considered as a feature vector containing normalized distances, angles, and scales. In fact, the training samples are fabricated by relationships between boundaries fragments as the local features. Figure 5 shows an example of this concept. Blue lines specify the relation between boundary fragment 1 and other boundaries fragments. In the same way, red lines specify the relation between boundary fragment 4 and the others. We calculate the length of the lines, the angles between the fragments, and the scales of the fragments.

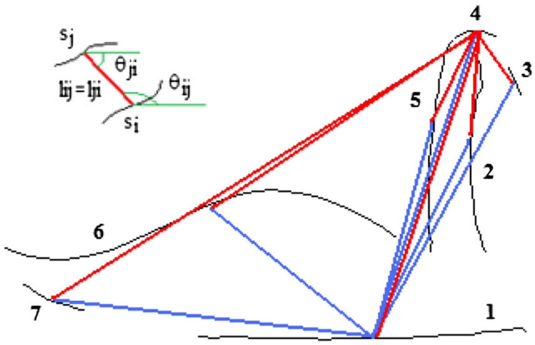

Fig. 5 Relation between parts 1 and 6 with boundary fragments of the codebook for swan. *Numbers* denote codebook classes

The observation O contains o_t which is extracted from the relation matrix R as defined in Eq. (7).

$$R = \begin{bmatrix} (s_1, l_{11}, \theta_{11}) & (s_2, l_{12}, \theta_{12}) & \dots & \dots & (s_n, l_{1n}, \theta_{1n}) \\ (s_1, l_{21}, \theta_{21}) & (s_2, l_{22}, \theta_{22}) & \dots & \dots & (s_n, l_{2n}, \theta_{2n}) \\ \dots & \dots & (s_i, l_{ij}, \theta_{ij}) & \dots & \dots \\ \dots & \dots & \dots & \dots & \dots \\ (s_1, l_{n1}, \theta_{n1}) & (s_2, l_{n2}, \theta_{n2}) & \dots & \dots & (s_n, l_{nn}, \theta_{nn}) \end{bmatrix} \tag{7}$$

$$\begin{aligned} &R(:) = [R(1,:), R(2,:), \cdots, R(n,:)] \\ &o_t = \text{ No redundant form of } (R(:)) \\ &\quad \text{and removed the zero values} \end{aligned}$$

In this matrix, n shows the number of boundary fragment of interested object or number of clusters in the codebook. s_i indicates the normalized scale (or length) of the ith boundary fragment, which is normalized by summation over all scales. l_{ij} is the length of line that connects the edge fragments i and j, which is normalized by summation over all line lengths, and θ_{ij} is the angle of this line, which is normalized by dividing to 2π. As we see in Eq. (7), dimension of the observation vector is dependent to the number of fragments. In fact, to construct the relation vector o_t, we need to consider all scales (or lengths) of fragments, all mutual distances of fragment pairs and all mutual angles between fragment pairs. Considering that $l_{ij} = l_{ji}, \theta_{ji} = \pi - \theta_{ij}$, we eliminate the duplicated parameters from o_t to remove redundant features. Also, we use each s_i one time and remove l_{ii}, θ_{ii} from o_t because they are always zero and have no valuable information.

After constructing the observation collection $O = \{o_t, t = 1\ldots T\}$ based on boundary fragments relationships of image samples $\{im_t, \ t = 1\ldots T\}$, we use them to train GMM. Dimension of the GMM is selected as dimension of o_t which depends on the number of fragments. For example, if the object contains 3 number of boundary fragments, dimension of GMM will be 9 as illustrated at the following:

$$\begin{aligned} R &= \begin{bmatrix} (s_1, l_{11}, \theta_{11}) & (s_2, l_{12}, \theta_{12}) & (s_3, l_{13}, \theta_{13}) \\ (s_2, l_{21}, \theta_{21}) & (s_2, l_{22}, \theta_{22}) & (s_2, l_{23}, \theta_{23}) \\ (s_3, l_{31}, \theta_{31}) & (s_3, l_{32}, \theta_{32}) & (s_3, l_{33}, \theta_{33}) \end{bmatrix} \\ &\Rightarrow \\ R(:) &= [s_1, l_{11}, \theta_{11}, s_2, l_{12}, \theta_{12}, s_3, l_{13}, \theta_{13}, s_2, l_{21}, \theta_{21}, s_2, \\ &\quad l_{22}, \theta_{22}, s_2, l_{23}, \theta_{23}, s_3, l_{31}, \theta_{31}, s_3, l_{32}, \theta_{32}, s_3, l_{33}, \theta_{33}] \\ l_{ij} &= l_{ji}, \theta_{ji} = \pi - \theta_{ij}, l_{ii} = 0, \theta_{ii} = 0, \\ &\Rightarrow \\ o_t &= [s_1, s_2, s_3, l_{12}, l_{13}, l_{23}, \theta_{12}, \theta_{13}, \theta_{23}] \\ &\Rightarrow \\ D &= 9 \end{aligned}$$

The number of mixtures of GMM is selected arbitrarily. We use 2 Gaussian mixtures because low complexity leads to higher training speed. Furthermore, the acceptable results are obtained by 2 Gaussian mixtures. To train the GMM, the parameters of λ are estimated by maximizing the log-likelihood function $\log p(O|\lambda)$ using the maximum likelihood estimation (MLE) by EM algorithm.

3.3 Generic model descriptor

In this subsection, we propose an extra process of object model construction that we use it to remove the False Positives. False Positives are occurred in images when some instances are detected and inferred as interest object incongruously. Therefore, a known model of the object is required to remove such incorrect detections.

As discussed before, the class-specific codebook contains boundary fragments. We select a fragment from each cluster of the codebook that has the mean scale and angle, call them representative fragments (or center of clusters), and link them to extract the outline of the object. The sequences of representative fragments are linked manually in an order to make the shape of the object proper. This order will be used in detection stage to extract shape of the object in the test image. Besides, the parameters of fragments such as angle, length, and position in reference to the center of object are useful to determine the linking order in the detection stage. For example, as illustrated in Fig. 6, the model of swan is extracted by connecting the boundary fragments in the order of: (F_1, F_2, F_3, F_4, F_5, F_6, F_7, F_1), where F_j represents the feature vector of the fragment j.

We fill inside the constructed contour and make a binary image of the object. Then, we solve the Poisson equation on this image. In fact, the solution of the Poisson equation on the binary image represents the object shape by propagating the boundary contour of the object to every internal pixel [26]. The shape of the object may not be extracted completely in natural images because of their complex background. Then, the Poisson equation solution of the detected object may not be same as the Poisson equation solution of the model. Therefore, the solution of Poisson equation is not appropriate for using in the False Positive removing process for detection task. To get more robust generic model of object, we use the local orientations. The local orientations of the object are obtained by computing Eigen vector corresponding to the smaller Eigen value of Hessian matrix of the Poisson equation solution (U) in all of the pixels inside the model (See Eq. 2). To simplify this representation, we quantize the local orientations values to six quantities, 0, 90, ±30, and ±60 so that we are able to find a simpler description and use it as the generic model of the object. Figure 6 shows the extracted shape (top left),

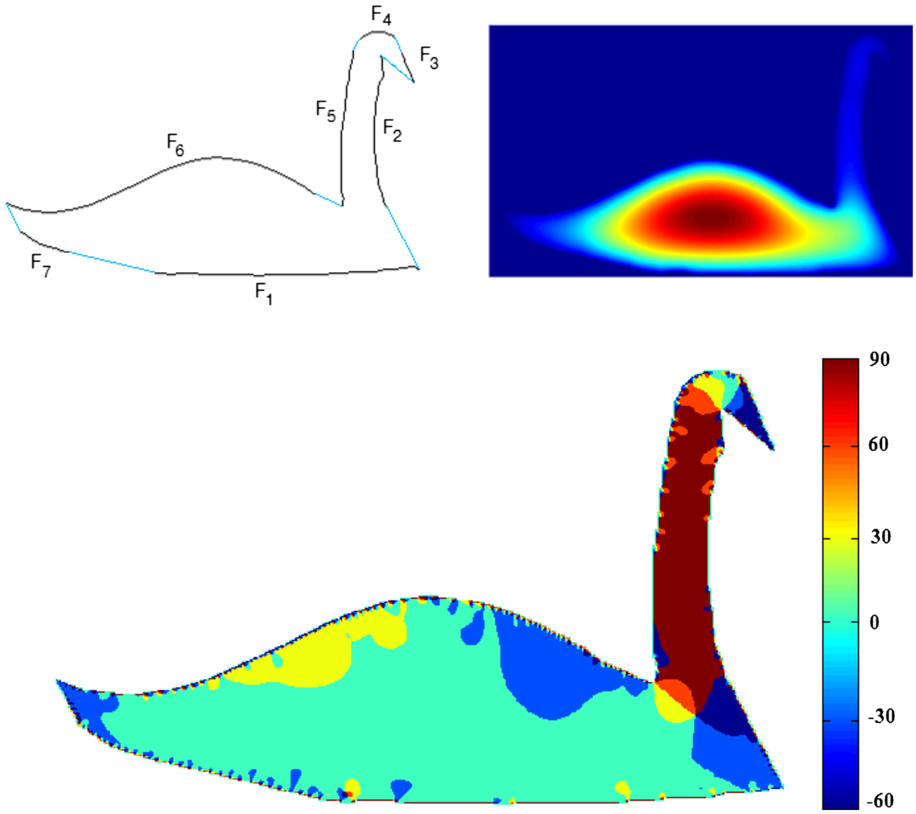

Fig. 6 Generic model of the object. *Top left* is a generic shape extracted by linking the representative fragments. *Top right* is the solution of Poisson equation on the shape. *Bottom* is the big view of the generic model of the object. *Colors* indicate quantities of local orientations (color figure online)

the solution of the Poisson equation (top right), and the generic model of the object (bottom). In this generic model, the local orientations of each region are shown with different colors. For example, the green color region inside the model indicates the angle of 0°, and the brown color in the region of the neck specifies the angle of 90°.

To extract the shape feature, we divide the generic model to multiple patches and obtain the histogram of local orientation in each patch (See Fig. 7). Histograms are used to match the model to the detected objects (we use 16 patches). They contain information about the local orientation of the object. Each bar in a histogram represents the number of quantized local orientations that are normalized by the quantity of the corresponding bar of the whole object histogram (H_T). The feature vector of the model is presented as follows:

$$H = \left(\frac{h_1}{h_{T1}}, \frac{h_2}{h_{T2}}, \ldots, \frac{h_{16}}{h_{T16}}\right) \tag{8}$$

$$h = \left\{N_{-\frac{\pi}{3}}, N_{-\frac{\pi}{6}}, N_0, N_{\frac{\pi}{6}}, N_{\frac{\pi}{3}}, N_{\frac{\pi}{2}}\right\}$$

In Eq. (8), h_T is the histogram of the local orientation of the Poisson equation of the whole object, $h_{1,2,\ldots,16}$ constitute the histogram of the local orientation of the Poisson equation of the 16 patches. N represents the quantities of the bars of the histogram. The image dataset contains the binary images of the object in natural images. We match the histogram of local orientation came from the solution of Poisson equation for binary shape with the histogram of the generic model.

4 Object detection

In the object detection stage, we try to find the interested object in the image. The proposed object detection process as is illustrated in flowchart of Fig. 2 is divided into 3 steps:

1. Localizing objects in the most probable regions: in this step, we extract the boundary fragments of the test image and match them to the entries of the codebook.
2. Finding objects boundaries: the candidate boundary fragments are then applied to the trained GMM model, and the object configuration is extracted by finding the object boundaries from the candidate boundary fragments.
3. False Positives elimination: False Positives are removed by matching the generic shape model with the extracted shapes.

4.1 Localizing objects in the most probable regions

In Sect. 3, we have represented the shape of an object as a set of boundary fragments. Each fragment was defined with a specific shape, location, and scale that are stored in a

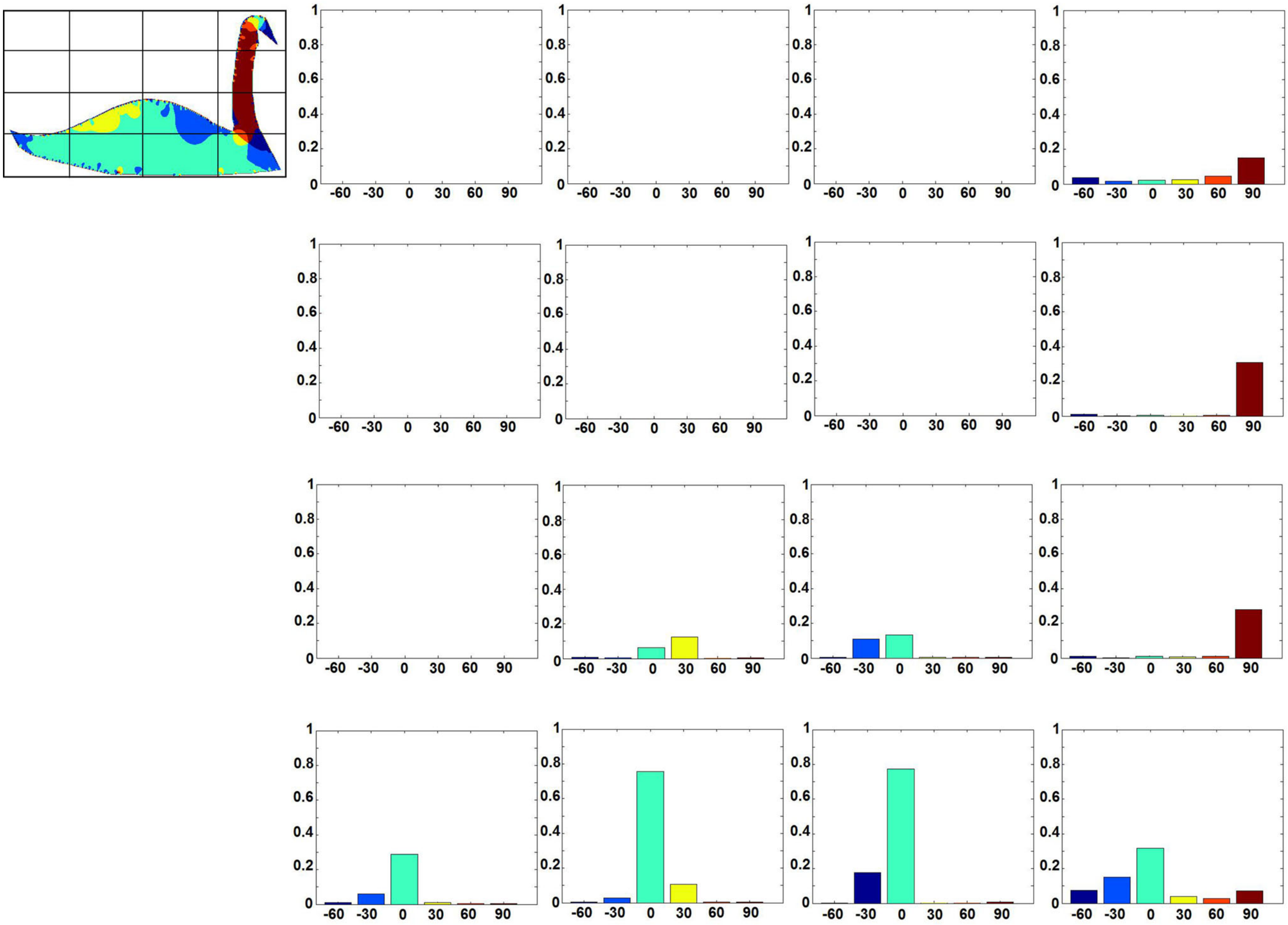

Fig. 7 Patches and *histograms* of a generic shape model. Each *bar* is normalized by the number of pixels in a patch

clustered codebook. In the first step of detection stage, as a similar method to training stage, the feature vector of edge fragments of test image is constructed by solving the Poisson equation on the edges, computing Eigen vector of the smallest Eigen value of Hessian matrix of the Poisson equation solution, disconnecting them from the high curvature places, and quantizing the orientations. Then, we match the edge fragments of test image with the fragments in the codebook based on their shape similarities given in Eq. (9). In this equation, F^a is an edge fragment in the codebook, and F^b is an edge fragment in the test image.

$$\begin{aligned} D\left(F^a, F^b\right) &= 1 - \frac{\left\langle \vec{\theta}^r, \vec{\theta}^a \right\rangle}{\left\|\vec{\theta}^r\right\|\left\|\vec{\theta}^a\right\|} \\ &= 1 - \frac{\theta_{\mathrm{l}}^a\theta_{\mathrm{l}}^b + \theta_{\mathrm{r}}^a\theta_{\mathrm{r}}^b}{\sqrt{\left(\theta_{\mathrm{l}}^a\right)^2 + \left(\theta_{\mathrm{r}}^a\right)^2}\sqrt{\left(\theta_{\mathrm{l}}^b\right)^2 + \left(\theta_{\mathrm{r}}^b\right)^2}} \end{aligned} \tag{9}$$

More precisely, an edge fragment of test image is considered to be a match of a codebook fragment if $D < 0.2$. Since a pair of the matched edge fragments induces a translation and scale transformation, each match votes for the presence of an object boundary at a particular location. Votes are weighted by 1-D so that the more similar edges contain more weights. We make the vote scale invariant by the following equations:

$$\begin{aligned} x_h &= x_{ct} + \Delta x \cdot \frac{S_t}{S} \\ y_h &= y_{ct} + \Delta y \cdot \frac{S_t}{S} \end{aligned} \tag{10}$$

In Eq. (10), x_h and y_h are the position of the vote in Hough voting space, x_{ct} and y_{ct} define the center of the edge fragment, Δx and Δy explain the position of the boundary fragment with respect to the object center stored in the codebook, S_t is the length of test image fragment and S is the length of boundary fragment in the codebook.

Variation of color for each pixel suggests different regions in the image and could be used as a feature to find the regions belonging to the objects. In fact, object boundaries can be considered as the edges between the regions with high color (or intensity) difference. We call such strong edges as the effective edges. Effective edges could be extracted using a high threshold in the gradient of the image and decomposed

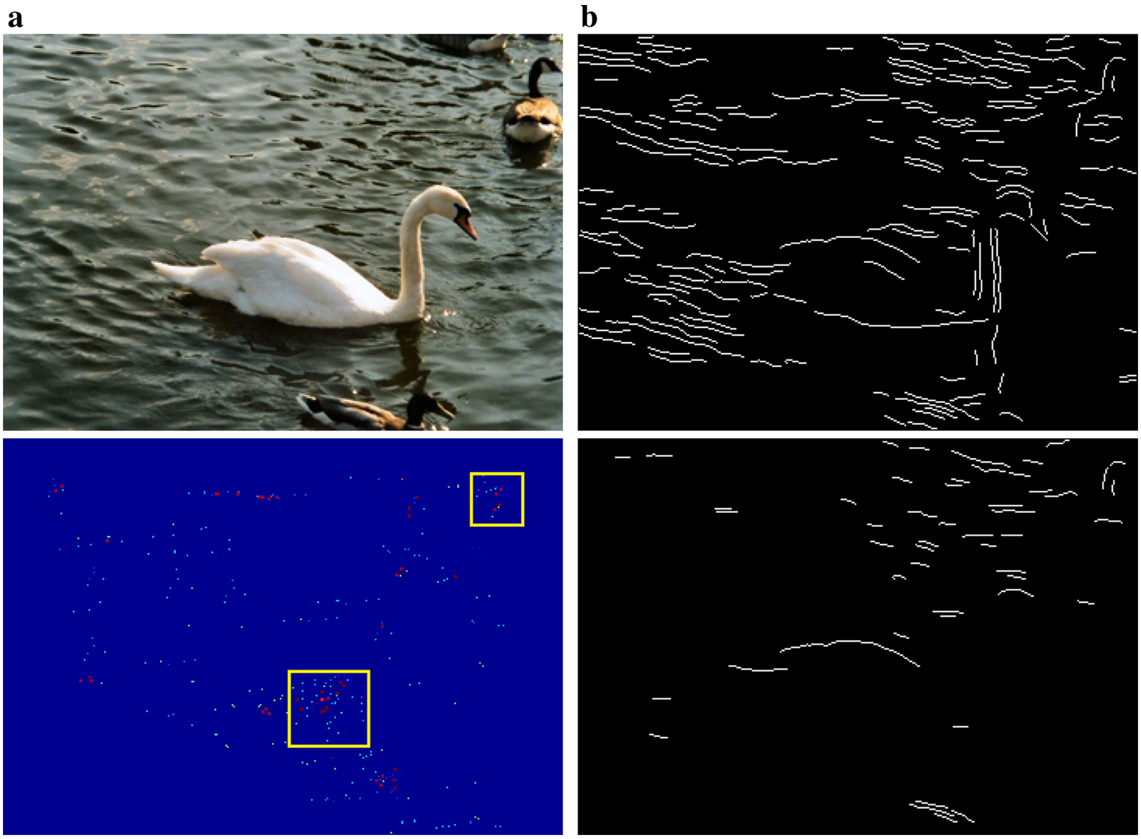

Fig. 8 Hough voting space and edge fragments. **a** An image of the swan and Hough voting space. *Yellow rectangle* shows the regions established by Mean-Shift. **b** Edge fragments and effective fragments of the image (color figure online)

to fragments as discussed before. Effective edge fragments are used to vote for the object presence with the higher weight. The object center is obtained by seeking the local maximum regions in Hough voting space. We use Mean-Shift algorithm [14] to find the regions that have enough total weights and votes. The local maximums in the voting space define rough estimates of the location and scale of the candidate object instances [14]. Figure 8 shows the local maximum that has been obtained by the boundary fragments. The Local maximums with the value higher than a threshold are preserved, and the others are removed.

4.2 Finding object boundaries

The above voting procedure delivers some local maximums in a typical cluttered image, as the local features are not very distinctive. However, it could localize the objects in the most probable places of the image. In this subsection, we obtain the relationship between the boundaries to detect the object in cluttered natural images where unrelated fragments may vote for the object presence and be considered as the object boundaries, by mistake.

Object configuration can extract the shape of the object using the relation between the boundary fragments and remove the outliers. We use the trained GMM to extract the proper fragments to specify the object boundaries from the set of inliers and outlier boundary fragments.

To use the GMM in the detection stage, a set of test observations, o_t, must be created. To achieve this end, we select the associated fragments in each detected region by Mean-Shift. Different subsets of the associated fragments are picked and the relations between them are computed and so the test observations are created. The MLE evaluates the quality of the correspondence of the test and train observations [28]. Large amounts of MLE give the proper boundaries fragments and remove the outliers. Figure 9a shows the extracted boundary fragments in an image.

4.3 False Positives elimination

In the previous subsection, we extracted the fragments as the object boundaries. However, in cluttered images, some instances may be found as outliers in different regions of an image because of finding similar edge of test image to the local boundary fragments stored in the codebook. It leads to a false explanation of the objects in images, which is referred to as False Positives.

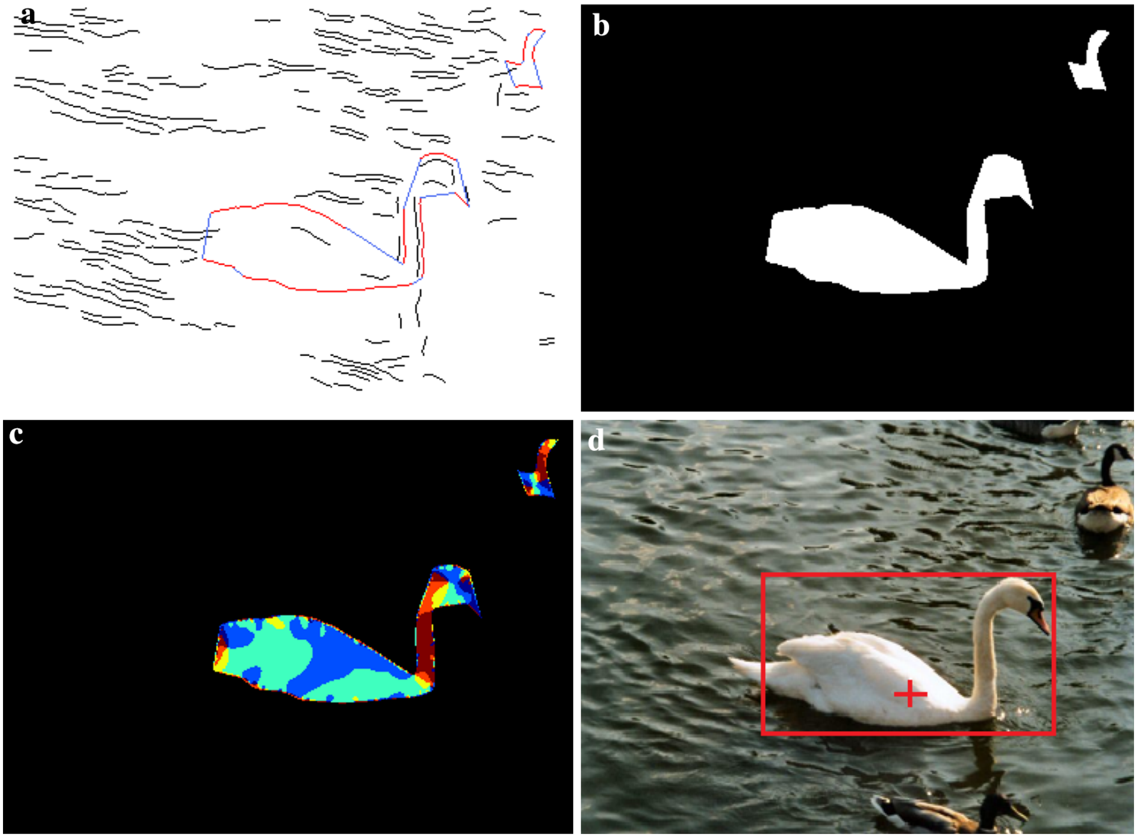

Fig. 9 Shape explanation. **a** Edge fragments of image. *Red edges* represent boundary fragments extracted by GMM and *blue edges* represent boundary fragments connection. **b** Extracted binary shape from image. **c** Local orientation of binary shape for evaluating histograms and matching with generic model in Fig. 7 to remove false positives. **d** Detected object (color figure online)

To extract the shapes of the objects, we connect all the boundary fragments in detected regions that have been taken from GMM. We connect them by a sequence that was specified in the Generic Model Descriptor in Sect. 3.3 in order to extract the object shape. By connecting the boundary fragments and filling inside of the connected regions, we construct a binary shape, which is utilized for the matching process.

We solve the Poisson equation on the binary images and extract the local orientations of the object. Histograms of the local orientations are computed for each patch as the procedure that was discussed in Sect. 3.3, and used for matching. If the value of C be obtained more than a threshold, it will be considered as False Positive and so will be removed.

Figure 9 shows the detected object after pruning False Positives. We show the detected object by a bounding box that covers the object and a plus sign, +, which lies in the center of the extracted region by Mean-Shift algorithm.

5 Experimental results

We present an extensive evaluation of our method using seven object classes from three challenging datasets, ETHZ, Weizmann, and INRIA horses. The capability of the shape extraction and the object detection in images, both in terms of bounding boxes and binary shapes, is measured. Our results were obtained after removing the False Positives. Detection results are compared with other state-of-the-art methods. We have demonstrated the results in each database, separately.

5.1 ETHZ database

This database contains a total number of 255 images in five diverse classes; i.e. bottles, swans, mugs, giraffes, and apple logos [29]. It is highly challenging, as the objects

Table 1 Number of training and test images for experiment on ETHZ dataset

Classes	Apple logos	Bottles	Giraffes	Mugs	Swan
Training natural images	20	24	44	24	16
Test pos.	20	24	44	24	16
Test neg.	215	207	167	207	223

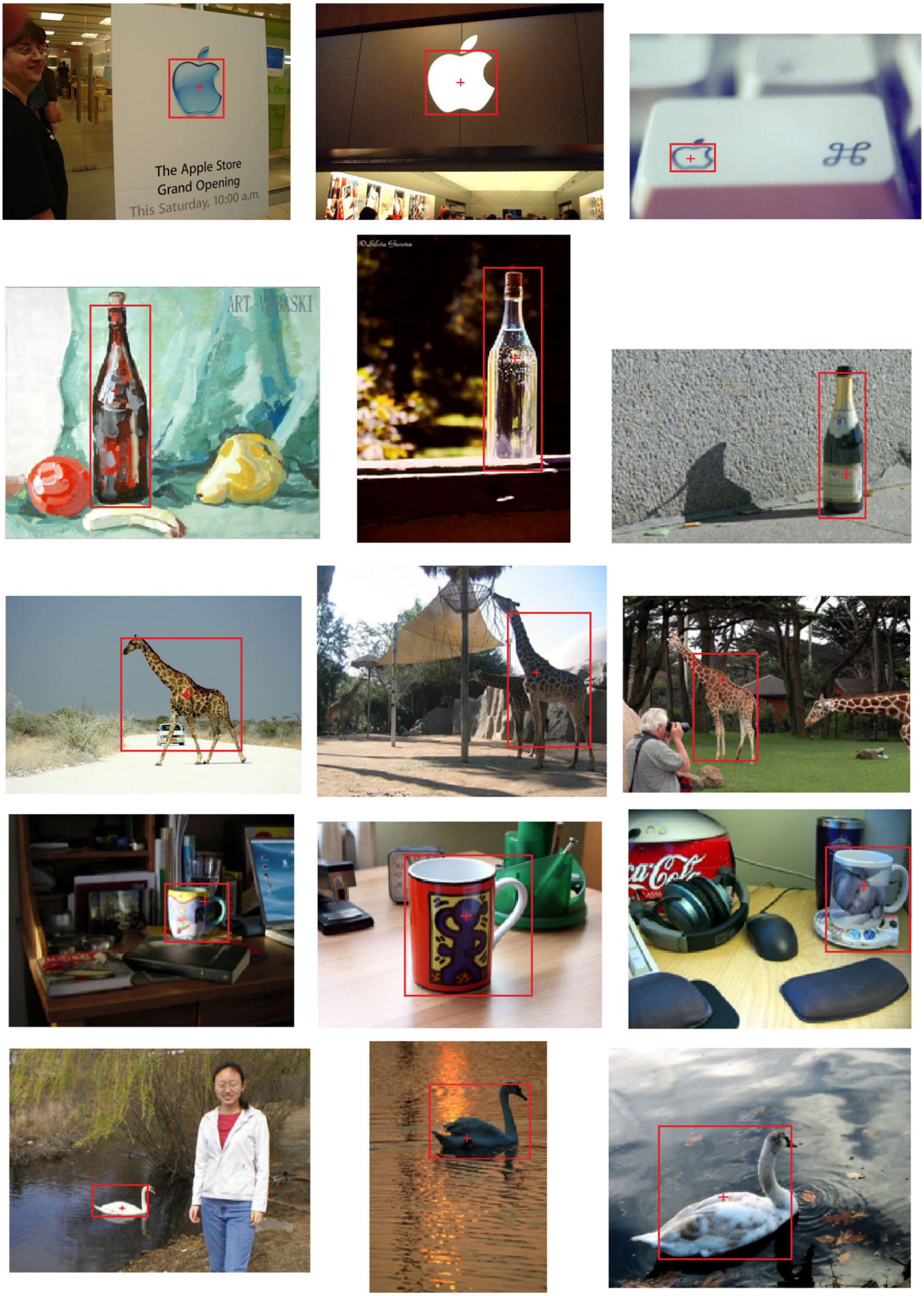

Fig. 10 Examples of detected objects. All of the objects are from ETHZ dataset. Detected objects are shown by a bounding box

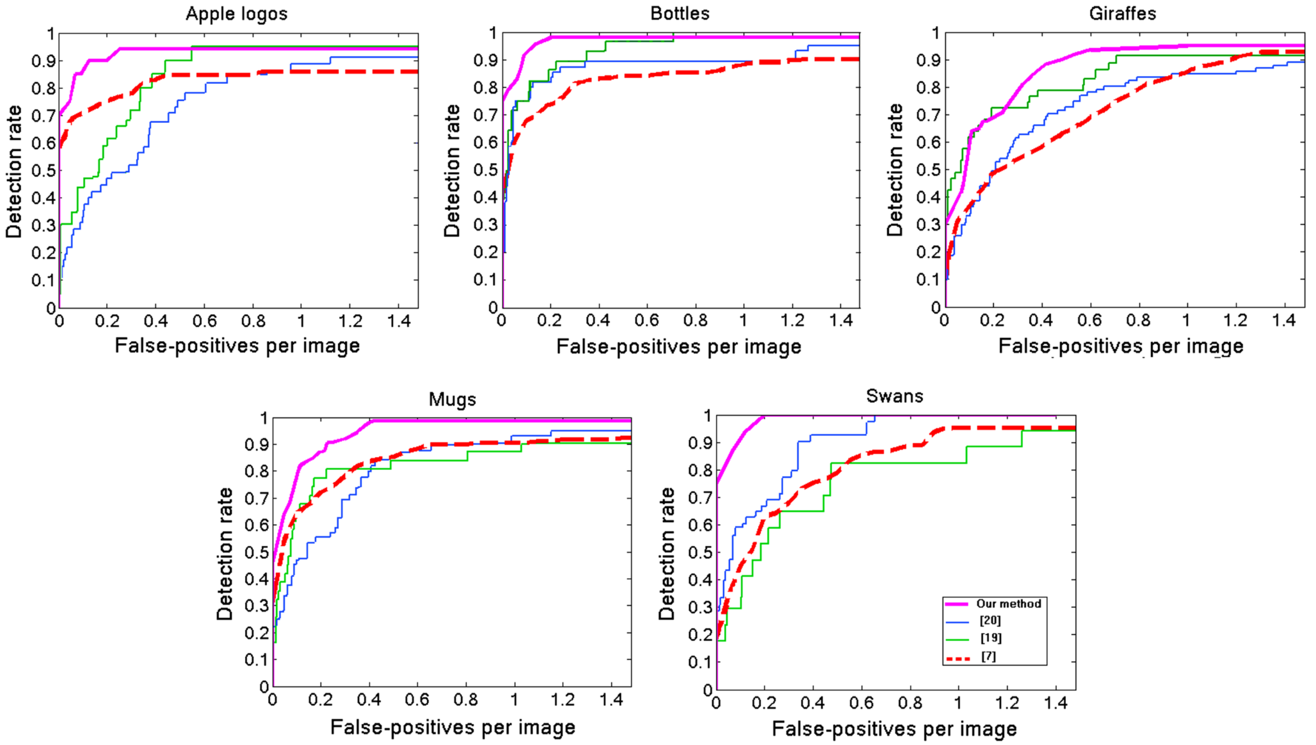

Fig. 11 Object detection results. Each plot shows four curves which have been extracted under the 20 % IoU criterion. *Magenta curves* show performance of our method. *Blue*, *green* and *dotted red curves* show performances of methods in [21], [20] and [7], respectively (color figure online)

Table 2 Comparison between detection rates of different methods according to plots in Fig. 11, under 20 % IoU criterion

Detection rates in 0.3/0.4 FPPI				
Classes	Our method	Method of Ferrari et al. [21]	Method of Ferrari et al. [20]	Method of Ferrari et al. [7]
Apple logos	0.96/0.96	0.568/0.728	0.65/0.832	0.777/0.85
Bottles	0.98/0.98	0.891/0.91	0.893/0.893	0.814/0.832
Giraffes	0.8/0.878	0.626/0.67	0.723/0.787	0.523/0.586
Mugs	0.92/0.98	0.70/0.78	0.80/0.8	0.781/0.836
Swan	1/1	0.72/0.9	0.647/0.647	0.68/0.754
Average	0.91/0.951	0.70/0.798	0.743/0.792	0.715/0.772

appear in a wide range of scales. It is considerable that many images are severely cluttered with disturbing edges and objects comprising only a fraction of the total image area. We evaluate the performance of our method in detecting objects of this database by comparing our results with those of Ferrari et al. methods in [7, 20, 21, 30].

We used half of the images in each class for obtaining object descriptors. Our method does not require any negative images for training. The test set consists of all other images in the dataset. The test images in a class are used as a positive test for own class and as a negative test for other classes. The negative images are used to estimate False Positive rates. Table 1 shows the number of training and test images. Figure 10 shows some examples of the detected objects of this database.

We compare the proposed method with the results in [7, 20, 21] under similar conditions. The number of the selected images is the same as the number of training and test images in those papers. An object was detected by 20 % IoU (Intersection of Union) criterion described in [21]. Under this condition, the detection is counted as positive if the object bounding box overlapped more than 20 % with the ground truth; otherwise, it is identified as a False Positive. Figure 11 shows the plots of the detection rate against the number of False Positives. In [20], a hand-plotted model was used to detect the objects of each class.

Table 3 Comparison between detection rate of [30] and our method under 80 % IoU criterion without testing on negative images

	Bottles (%)	Giraffes (%)	Swans (%)
Our method	85	60	89
Method of Adluru and Latecki [30]	80	45.45	87.5

Detection rates in 0.3 and 0.4 False Positives per Image (FPPI) represent the performances of methods. As the plots show, the results of our method are better than the others according to the detection rate in 0.3 and 0.4 FPPI.

Our method does not use discriminative learning like Ferrari et al. [21]. It is obtained only from the positive images. Models in our experiments are the average shape of half of the objects in each class. Thus, they include rich information about the shape of the objects. Furthermore, it reveals the power of our method that can make worthwhile detection results without employing negative images in training stage. In [20], a hand-plotted model was used to extract shapes from images. The relation between the boundary fragments can model the shapes of the objects, but TPS-RPM algorithm in [7] may match a model to the disturbing edges and cause False Positives. We removed the False Positives as described in Sect. 4 to detect the objects correctly. This led to better results, as compared with those of other studies. The results of the detection rate in 0.3 and 0.4 False Positive per image are presented in Table 2.

In [30], an object is detected by grouping boundaries and detection succeeds if bounding box overlaps more than 80 % with ground truth. In the mentioned work, FPPI is not reported. To compare with [30], we evaluate our method over three classes of database. We use half of the images in each class for training and the remainder for test. Method in [30] uses a simple hand-plotted model to form the shape of the object. Table 3 shows results of our method and [30] which demonstrates our proposed method makes better results than the compared one.

We compare our method with [7, 31, 32] by evaluating PASCAL criterion. Under this condition, an object is detected if bounding box overlaps more than 50 % with ground truth. The number of selected images for training and test images is the same as Table 1. Figure 12 shows the plots of detection rate against the False Positives per image of proposed method and methods of [7, 31]. Detection rates in 0.3 and 0.4 False Positives per image are shown in Table 4. As these tables show, our method has the best performance in four classes (apple logos, bottles, mugs and swan). Because of the clutters in giraffe images and textures of giraffe body, our method has the less detection rate in comparison to [31] in giraffe class, because edge samples or geometric blur feature is not sensitive face to edge breaking. Figure 13 illustrates the recall against precision

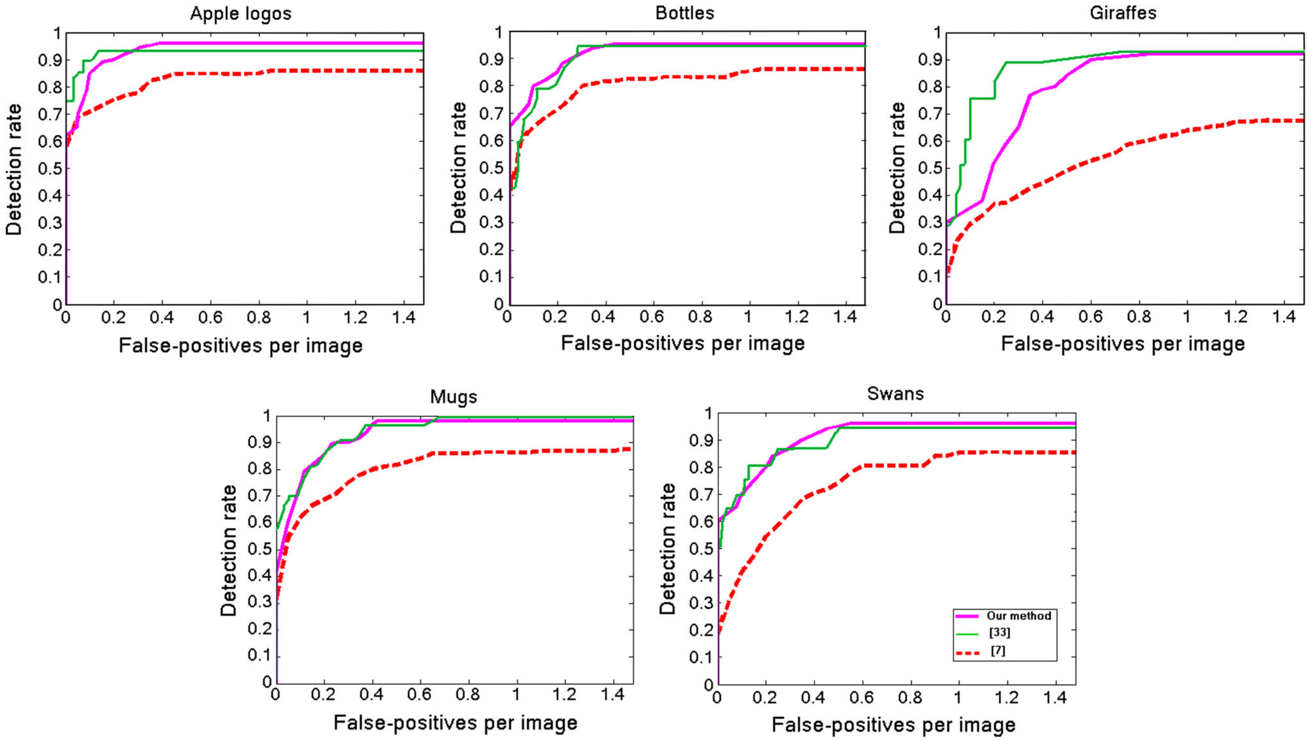

Fig. 12 Comparison of object detection rates under PASCAL criterion. *Magenta curves* show performance of our method. *Green* and *dotted red curves* show performances of methods in [31] and [7], respectively (color figure online)

Table 4 Comparison between detection rates of different methods according to the plots in Fig. 12, under PASCAL criterion

Detection rates in 0.3/0.4 FPPI			
Classes	Our method	Method of Maji and Malik [31]	Method of Ferrari et al. [7]
Apple logos	0.93/0.96	0.95/0.95	0.75/0.8
Bottles	0.98/0.98	0.93/0.964	0.75/0.8
Giraffes	0.62/0.78	0.896/0.896	0.37/0.42
Mugs	0.936/0.98	0.936/0.967	0.7/0.77
Swan	0.85/0.9	0.85/0.85	0.55/0.68

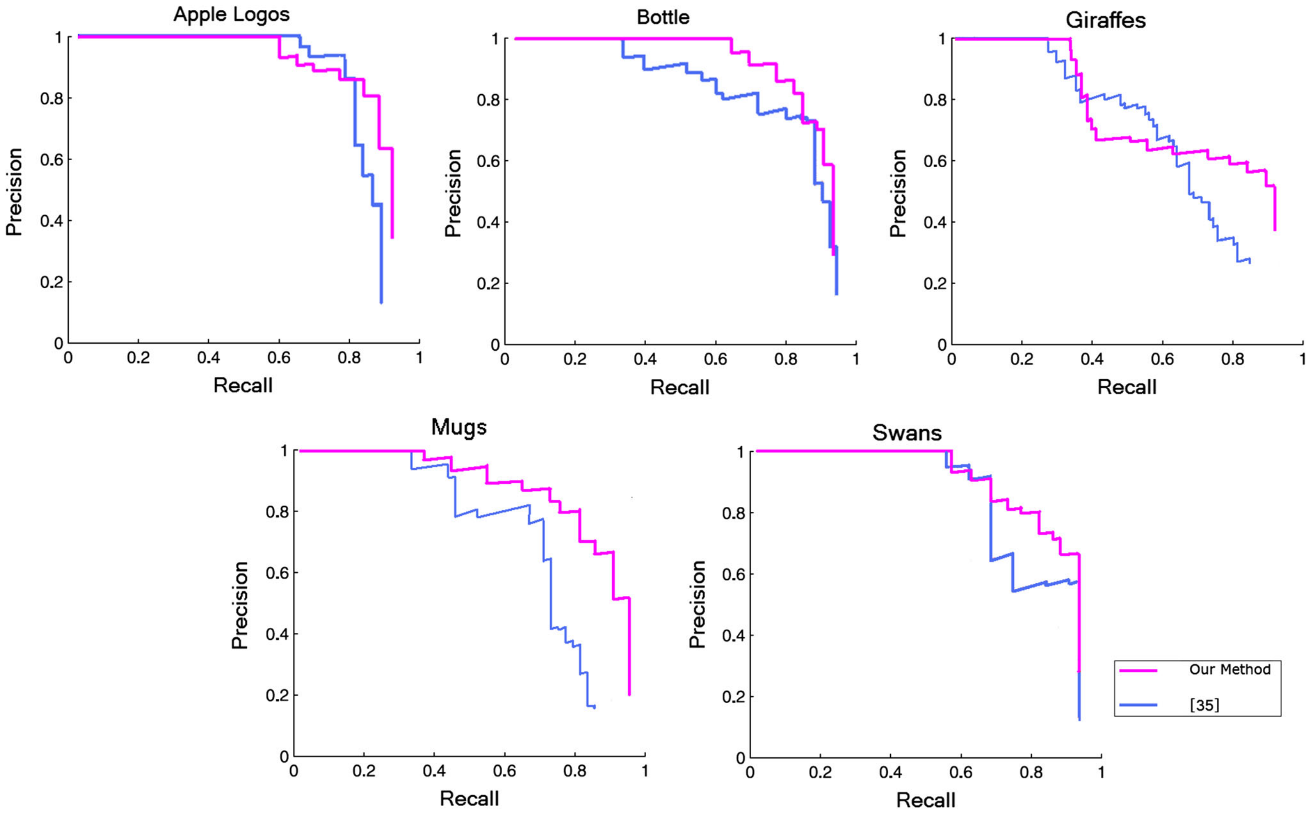

Fig. 13 Comparison of object detection under PASCAL criterion by recall-precision curve between proposed method and [32]. *Magenta curves* show performance of our method. *Blue curves* show performance of methods in [32] (color figure online)

to compare the proposed method with [32]. In [32], object boundary bundles are extracted to vote for the object location and K-NN is used to find optimal fragment bundle correspondence. To detect the object, they evaluate shape context distance and combine shape information with appearance. Their method requires negative training samples in contrast to our method that does not require any negative training samples. The method in [32] is plotted with blue color and our method is plotted with magenta color. As the plots show, the proposed method has better results at overall.

Comparing the detection results between different classes show that the proposed method gives the best results in swans' class because the images in this class are simple and the disturbing edge fragments does not influence the object's boundaries. Giraffe's class consists of cluttered images because of the natural environment. Giraffes are camouflaged by a texture that breaks boundary edges. Pose variation and articulated movements are another problem in this class. Therefore, it contains the lowest detection rate. Mugs have labels or shapes on their body, which disturb object boundaries, so, in such cases, the detection rate is somewhat low.

5.2 INRIA horses

This dataset [33] consists of 170 images of horses from right-view side. The number of the horses is more than one

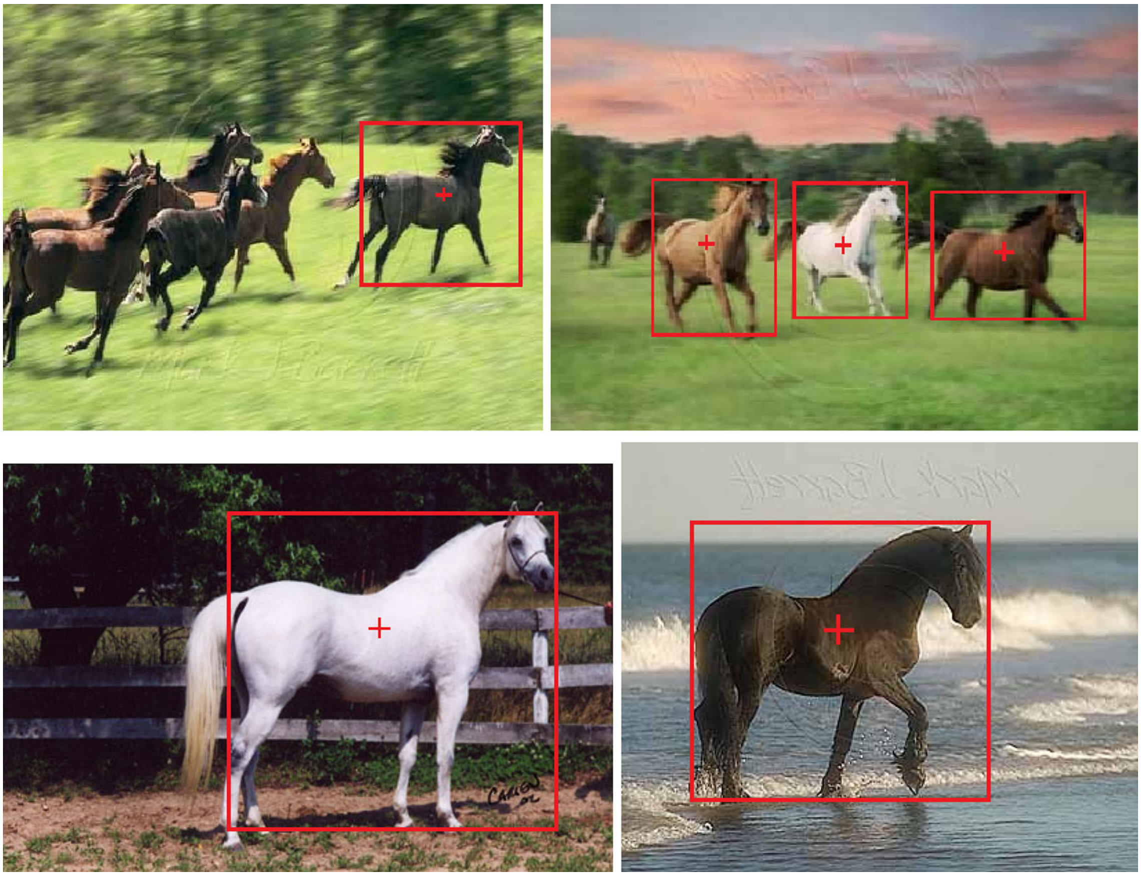

Fig. 14 Examples of detected objects in INRIA horse dataset by our proposed method

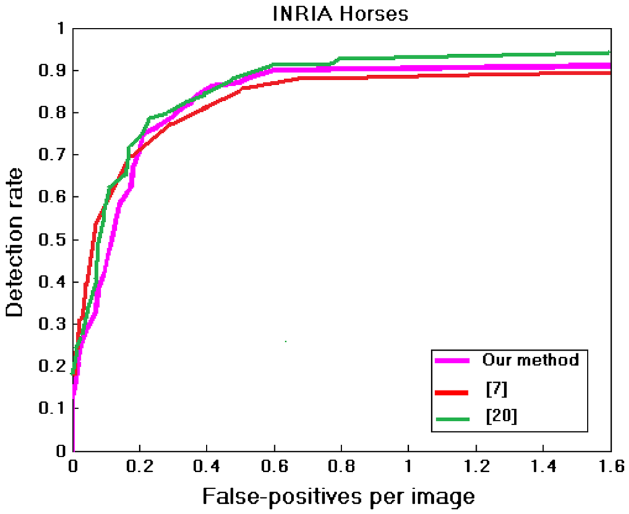

Fig. 15 Detection rate versus false positive per image for INRIA horses dataset. This plot shows performance of our method (*magenta*) against [7] and [21] under 20 % IoU criterion (color figure online)

Table 5 Comparisons results in INRIA horses detection under 20 % IoU criterion

Detection rates in 0.3/0.4 FPPI		
Our method	Ferrari et al. [21]	Ferrari et al. [7]
0.8/0.855	0.84/0.85	0.78/0.8

in some images. They contain different colors and textures and articulated movements in cluttered images. Some detected samples of this dataset are illustrated in Fig. 14. As conditions in [7] and [21], we selected 50 natural images for the training stage and the remaining 120 natural images for the detection stage. Detection performance in these papers is reported in 20 % IoU criterion better than PASCAL. We used 170 negative images for the test and False Positive estimation. We evaluated the results by 20 % IoU criterion and showed them in detection rate versus False Positive per image curve. Figure 15 shows this plot. Table 5 demonstrates the results of our method, [7] and [21] in 0.3 and 0.4 FPPI. As this table shows, our results are close to them. However, our algorithm has better detection results in 0.4 FPPI of this dataset. The variation in the poses of the horses in some images causes faults in detection.

5.3 Weizmann horses dataset

This dataset consists of 328 images of horses from a left-side view and their silhouettes [34]. They contain different

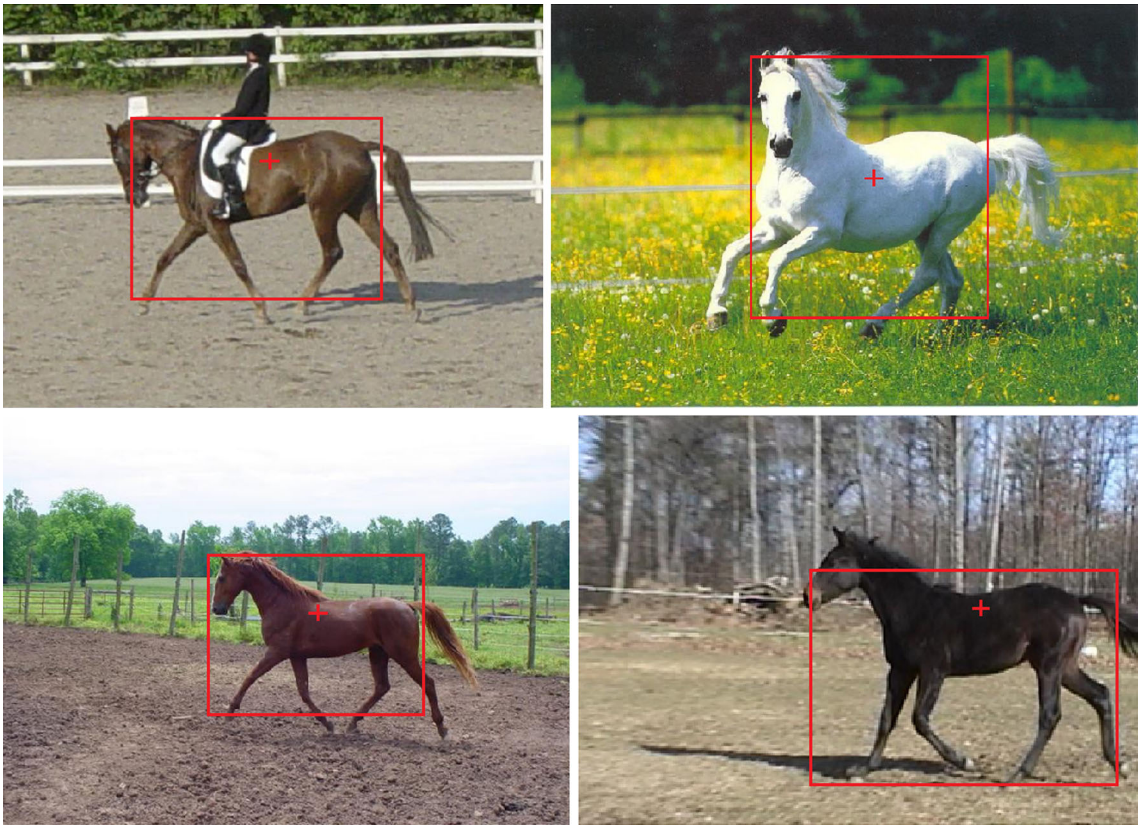

Fig. 16 Examples of detected objects in Weizmann horse dataset by our proposed method

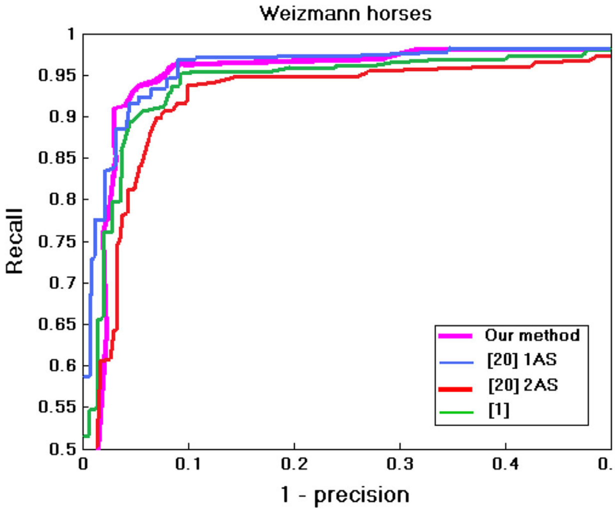

Fig. 17 Comparison of object detection using Weizmann horse dataset under 20 % IoU criterion by recall-precision curves between proposed method and [1, 21]. *Magenta curves* show performance of our method (color figure online)

Table 6 Comparisons of equal error rates (EER) of three methods obtained from experiment on Weizmann horses dataset

Our method	Method of Shotton et al. [1]	Method of Ferrari et al. [21]	
		PAS	1AS
0.938	0.921	0.917	0.935

colors and textures with various scales and articulated movements. Some samples of detected horses in this dataset are illustrated in Fig. 16. To compare our method against [1] and [21] in similar conditions, we chose the first 50 images of the dataset for the training stage. The test set consists of 277 positive and 277 negative images, collected from Caltech 101 [35] dataset.

We show the detection results in terms of recall-precision curve (RPC). The detection results in [21] are reported based on 20 % IoU criterion. Figure 17 shows the recall-precision plot of the detection results. As the plot shows, the recall-precision equal error rate (EER) is 0.938. In [21], equal error rates of 0.917 and 0.935 were obtained, respectively, by PAS and 1AS. In [1], an object is detected correctly if a peak lies within 25 pixels of correct Centroid (a circle with a radius of 25 pixels corresponds to 20 % of the average object size). This criterion is near to 20 % IoU. The detection method of [1] yielded a recall-precision EER of 0.921. Comparisons of the results are given in Table 6.

As the results show, our method has the good performance of object detection in this dataset. Horses in this dataset, like the ones in INRIA, have more distinctive colors from the background. Therefore, effective edges can help the detection process. Articulated movements of horses make faults in detection. On the other hand, the big parts of the horses such as the torso have invariant shapes, so they can be detected correctly. Figure 15 shows some examples of the detected horses from this dataset. We achieved better results in Weizmann dataset than in INRIA dataset, because some of the horses in INRIA images include occlusion and have been captured in different view directions. All of the images in Weizmann dataset consist of only one horse.

6 Conclusion

In this paper, a new method for object detection has been proposed. By novel object descriptors that we discussed, a codebook containing boundary fragments was created. Using GMM, we built relations between boundary fragments and extracted object configuration. The generic shape model of the object was extracted and the local histograms of orientation of Poisson equation were computed. We used Poisson equation to find fragments and generic model features. To detect objects, we extracted the most similar fragments of the test image with boundary fragments stored in a codebook that voted for the presence of the object in Hough voting space. Mean-shift algorithm was used to find the most probable regions of the object presence. Objects shapes were extracted by connecting the associated edges of these regions using learned GMM. False Positive is a usual fault that occurs in detection tasks. We proposed a procedure that removes False Positives. A better detection performance was achieved by the proposed False Positives elimination method. We used histogram matching for this reason where each histogram bin shows the number of the pixels in each local orientation of the object. We evaluated our method on three challenging datasets consisting of seven classes of objects. We compared our results with state-of-the-art methods. We illustrated the results through detection rate versus False Positive per image (FPPI) and recall versus precision curves. The experimental results confirmed the power of our proposed algorithm in object detection. The obtained detection results of the rigid objects were better than the non-rigid objects containing articulated movements. Since the swan class contains a specific pose of object without particular movements and also the images are not very cluttered, the best result was achieved in this class. The proposed method has some advancement against the object deformation. The minor deformations under single view like small articular or non-rigid variations are handled in our method because of quantizing the left–right orientation of boundary edge fragments to define their shape and using the GMM that makes possible tolerating of such minor changes. But, to handle the major deformation under single view, we need to train concurrent multiple models of object and design multi-object detection system. It is apparent that training of concurrent multiple models of object makes the detection system more vulnerable to outliers especially in the cluttered images. But there is still another solution for this problem and that is to detect different models of an object, separately. For example, when we want to detect a horse in image, we can first try to detect a side-view model of horse. If we were not able to detect a side-view horse model, we try, in the second attempt, to find front view model of horse and so on. This kind of detection is possible in our approach. It is enough to train the different shapes of object in different codebooks and try to find one of the shapes in different attempts. As a final point, while the proposed sophisticated system is complex in implementation but its power in facing with troubling edge fragments, removing the False Positives in cluttered scenes and providing better detection results compared to state-of-the-art methods makes the system worthwhile to computer vision community.

References

1. Shotton J, Blake A, Cipolla R (2008) Multiscale categorical object recognition using contour fragments. IEEE Trans Pattern Anal Mach Intell 30(7):1270–1281
2. Felzenszwalb PF, Huttenlocher DP (2000) Efficient matching of pictorial structure. In: Proceedings of IEEE Conference on computer vision and pattern recognition (CVPR'00), vol 2, pp 66–73
3. Agarwal S, Atwan A, Roth D (2004) Learning to detect objects in images via a sparse, part-based representation. IEEE Trans Pattern Anal Mach Intell 26(11):1475–1490
4. Burl M, Weber M, Perona P (1998) A probabilistic approach to object recognition using local photometry and global geometry. In: Proceedings of European Conference on computer vision (ECCV' 98), pp 628–641
5. Bouchard G, Triggs B (2005) A hierarchical part-based model for visual object categorization. In: Proceedings of IEEE Conference on computer vision and pattern recognition (CVPR'05), vol 1, pp 710–715
6. Leibe B, Leonardis A, Schiele B (2008) Robust object detection with interleaved categorization and segmentation. Int J Comput Vision 77(1–3):259–289
7. Ferrari V, Jurie F, Schmid C (2010) From images to shape models for object detection. Int J Comput Vision 87(3):284–303
8. Anvaripour M, Ebrahimnezhad H (2010) Object detection with novel shape representation using bounding edge fragments. In: Proceedings of International Symposium on telecommunication (IST'10), pp 846–851
9. Borenstein E, Malik J (2006) Shape guided object segmentation. In: Proceedings of the IEEE Conference on computer vision and pattern recognition (CVPR'06), vol 1, pp 969–976
10. Basri R, Costa L, Geiger D, Jacobs D (1998) Determining the similarity of deformable shapes. Vision Res 38:2365–2385

11. Garvilla D (2000) Pedestrian detection from a moving vehicle. In: Proceedings of European Conference on computer vision (ECCV'00), pp 37–49
12. Grauman K, Darrell T (2005) The Pyramid match kernels: discriminative classification with sets of image features. In: Proceedings of International Conference on computer vision (ICCV'05), vol 2, pp 1458–1465
13. Opelt A, Pinz A, Zisserman A (2006) A boundary-fragment model for object detection. In: Proceedings of European Conference on computer vision (ECCV' 06), pp 575–588
14. Leibe B, Schiele B (2004) Scale-invariant object categorization using a scale-adaptive mean-shift search. In: Proceedings of DAGM'04 Pattern Recognition Symposium
15. Belongie S, Malik J (2002) Shape matching and object recognition using shape contexts. IEEE Trans Pattern Anal Mach Intell 24(4):509–522
16. Chui H, Rangarajan A (2003) A new point matching algorithm for non-rigid registration. Comput Vis Image Underst 89(2–3): 114–141
17. Ommer B, Malik J (2009) Multi-scale object detection by clustering lines. In: Proceedings of International Conference on computer vision (ICCV'09), pp 484–491
18. Berg AC, Malik J (2001) Geometric blur for template matching. In: Proceedings of IEEE Conference on computer vision and pattern recognition, vol 1, pp 607–614
19. Geremy H, Gal E, Benjamin P, Daphne K (2009) Shape-based object localization for descriptive classification. Int J Comput Vision 84(1):40–62
20. Ferrari V, Jurie F, Schmid C (2006) Object detection with contour segment networks. In: Proceedings of European Conference on computer vision, pp 14–28
21. Ferrari V, Fevrier L, Jurie F, Schmid C (2007) Groups of adjacent contour segments for object detection. IEEE Trans Pattern Anal Mach Intell 30(1):36–51
22. Pham TV, Smeulders AWM (2005) Object recognition with uncertain geometry and uncertain part detection. Comput Vis Image Underst 99(2):241–258
23. Levin A, Weiss Y (2009) Learning to combine bottom-up and top-down segmentation. Int J Comput Vision 81(1):105–118
24. Sharon E, Galun M, Sharon D, Basri R, Brandt A (2006) Hierarchy and adaptivity in segmenting visual scenes. Nature 442: 810–813
25. Gorelick L, Basri R (2009) Shape based detection and top–down delineation using image segments. Int J Comput Vision 83(3): 211–232
26. Gorelick L, Galun M, Sharon E, Basri R, Brandt A (2006) Shape representation and classification using the Poisson equation. IEEE Trans Pattern Anal Mach Intell 28(12):1991–2005
27. Bergtholdt M, Kappes J, Schmidt S, Schnörr C (2010) A study of parts-based object class detection using complete graphs. Int J Comput Vision 87(1–2):93–117
28. Perronnin F (2008) Universal and adapted vocabularies for generic visual categorization. IEEE Trans Pattern Anal Mach Intell 30(7):1243–1256
29. ETHZ Database (2007) Ferrari V http://www.vision.ee.ethz.ch/datasets/downloads/ethz_shape_classes_v12.tgz. Accessed 2012
30. Adluru N, Latecki LJ (2009) Contour grouping based on contour-skeleton duality. Int J Comput Vision 83(1):12–29
31. Maji S, Malik J (2009) Object detection using max-margin Hough transform. In: Proceedings of IEEE Conference on computer vision and pattern recognition (CVPR'09), pp 1038–1045
32. Lu C, Adluru N, Ling H, Zhu G, Latecki LJ (2010) Contour based object detection using part bundles. Comput Vis Image Underst 114(7):827–834
33. Lear Data Sets and Images (2006-2013) LEAR-Learning and Recognition in Vision http://lear.inrialpes.fr/data. Accessed 2012
34. Weizmann Horse Database (2005) Borenstein E http://www.msri.org/people/members/eranb. Accessed 2012
35. Caltech101 Database (2006) Fei–Fei L, Fergus R, Perona P http://www.vision.caltech.edu/Image_Datasets/Caltech101/Caltech101.html. Accessed 2012